# Adsorption of nucleotides on biomimetic apatite: The case ofadenosine 5' triphosphate (ATP)

Khaled Hammami, Hafed El-Feki, Olivier Marsan, Christophe Drouet

# Adsorption of nucleotides on biomimetic apatite: The case of adenosine 5′ triphosphate (ATP)

Khaled Hammami [a,b], Hafed El-Feki [a], Olivier Marsan [b], Christophe Drouet [b,*]

[a] Laboratoire de L'Environnement et de Sciences de Matériaux (MESLAB), Faculté des sciences de Sfax, BP 802 3018 Sfax, Tunisia
[b] CIRIMAT Carnot Institute, UMR CNRS/INPT/UPS 5085, University of Toulouse, Ensiacet, 4 Allée E. Monso, 31030 Toulouse Cedex 4, France

ARTICLE INFO

*Keywords:*
Nanocrystalline apatite
Adenosine triphosphate
Adsorption
Nucleotide
Vibrational spectroscopy

ABSTRACT

ATP is a well-known energy supplier in cells. The idea to associate ATP to pharmaceutical formulations/biotechnological devices to promote cells activity by potentially modulating their microenvironment thus appears as an appealing novel approach. Since biomimetic nanocrystalline apatites have shown great promise for biomedical applications (bone regeneration, cells diagnostics/therapeutics, . . .), thanks to a high surface reactivity and an intrinsically high biocompatibility, the present contribution was aimed at exploring ATP/apatite interactions. ATP adsorption on a synthetic carbonated nanocrystalline apatite preliminarily characterized (by XRD, FT IR,Raman, TG-DTA and SEM-EDX) was investigated in detail, pointing out a good agreement with Sips isothermal features. Adsorption characteristics were compared to those previously obtained on monophosphate nucleotides (AMP, CMP), unveiling some specificities. ATP was found to adsorb effectively onto biomimetic apatite: despite smaller values of the affinity constant $K_S$ and the exponential factor $m$, larger adsorbed amounts were reached for ATP as compared to AMP for any given concentration in solution. $m < 1$ suggests that the ATP/apatite adsorption process is mostly guided by direct surface bonding rather than through stabilizing intermolecular interactions. Although *standard* $\Delta G^{\circ}_{ads}$ was estimated to only −4 kJ/mol, the large value of $N_{max}$ led to significantly negative *effective* $\Delta G_{ads}$ values down to −33 kJ/mol, reflecting the spontaneous character of adsorption process. Vibrational spectroscopy data (FTIR and Raman) pointed out spectral modifications upon adsorption, confirming chemical-like interactions where both the triphosphate group of ATP and its nucleic base were involved. The present study is intended to serve as a basis for future research works involving ATP and apatite nanocrystals/nanoparticles in view of biomedical applications (e.g. bone tissue engineering, intracellular drug delivery, . . .).

## 1. Introduction

Adenosine 5′ triphosphate (ATP) is a naturally occurring triphosphate nucleotide which is present in every cell. It consists of a purine base (adenine), ribose, and three phosphate groups linked through P—O—P linkages. Nucleotides were first recognized as important "elementary" molecules in metabolic interconversions, and then as the building blocks of DNA and RNA. More recently, it was found that nucleotides are also present in the extracellular fluid under physiological circumstances [1]. Extracellular ATP can then be broken down by a cascade of ectoenzymes and xanthine oxidase to form uric acid, which is finally excreted in urine.

The concept of "energy for cells" is often associated to ATP [2,3]: the hydrolytic transformation of ATP into ADP (adenosine diphosphate) and related loss of a phosphate ion ($HPO_4^{2-}$) is accompanied by the release of energy that can be used by cells for different metabolic processes (exothermic standard enthalpy change of $\Delta H^{\circ}_{hydrolysis} = -20.5$ kJ/mol at 298 K) [4,5].

Taking this "cell energy" storage role played by ATP molecules, the possibility to provide additional energy to cells by way of local delivery of ATP molecules appears appealing in the field of biomaterials/nanobiotechnologies. This could ultimately lead to imagine ATP-delivering (nano)systems, possibly associated to a concomitantly delivered drug. It may be mentioned also that, recently, an ATP-responsive anticancer drug delivery strategy has been reported, utilizing DNA-graphene crosslinked hybrid nanoaggregates as doxorubicin carriers, and showing the possibility to trigger the drug release upon interaction of the nanocarrier with ATP molecules [6].

* Corresponding author at: CIRIMAT Carnot Institute, "Phosphates, Pharmacotechnics, Biomaterials" Research Group, France.
*E-mail address:* christophe.drouet@ensiacet.fr (C. Drouet).

http://dx.doi.org/10.1016/j.apsusc.2015.11.100

The association of ATP with biomaterials/biotechnological engineered systems therefore appears as a novel potential strategy deserving specific attention in (nano)medicine (whether aiming at delivering directly ATP to cells or extracellularly). Since nanocrystalline apatites have shown great potential both in the field of bone regeneration [7–21] and for (intra)cellular applications (e.g. cancer diagnosis or therapy, . . .) [22–28], they were selected in the present study to examine the possible interaction existing between ATP and biomimetic apatite nanocrystals.

Generally speaking, nanocrystalline calcium phosphate apatites are characterized by an exceptional biological response as well as physico-chemical features similar to those of natural bone [11,29] allowing an increasing use in biomedicine. For example, it is used as a bioactive and osteoconductive bone substitute material in clinical surgery [30,31], and as a system for the delivery of drugs (e.g. [27,32,33]).

Synthetic nanocrystalline apatites represent a model for the basic constituent of the inorganic part of bones (65–75 wt.%, depending on age and sex) [11], with a general formula [34] $Ca_{10-x}(PO_4)_{6-x}(HPO_4$ or $CO_3)_x(OH)_{2-x}$ with $0 \leq x \leq 2$. These nanocrystals exhibit in particular special surface features as shown in previous investigations using spectroscopic techniques [35–40]: precipitated nanocrystals possess a prominent structured hydrated layer on their surfaces, which is gradually converted into more stable apatite domains during aging. This hydrated layer contains labile surface ions (e.g. $Ca^{2+}$, $HPO_4^{2-}$, $CO_3^{2-}$, . . .), leading to an exceptional surface reactivity either in terms of ionic exchanges or of molecular adsorption [7,15,16,18,25,41–49]. Interfacial properties play consequently a crucial role in calcified tissues and biomaterials. Generally, the adsorption of molecules on apatitic calcium phosphates mostly involves (potentially strong) electrostatic interactions.

In this study, the interaction between a biomimetic carbonated nanocrystalline apatite and ATP molecules was examined, especially with the view to determine and comment isothermal adsorption data. This study thus complements the investigation on the adsorption of nucleotides on biomimetic apatites: recently, the adsorption of adenosine monophosphate (AMP) [45] and cytidine monophosphate (CMP) [48] has indeed been explored, unveiling the role of the phosphate endgroup but also of the nature of nucleic base in such monophosphate nucleotides. Observations were also previously made on the effect of the presence of ATP molecules during the process of apatite precipitation [50]: ATP was then found to alter the apatite crystallization process through interaction with surface growth sites. This work is intended to serve as a preliminary standpoint study prior to the elaboration of any biomaterials/nanosystems associating ATP and biomimetic apatite.

## 2. Materials and methods

### 2.1. Starting materials

The biomimetic carbonated apatite sample, referred to as hac-7d, used in this work was prepared by a double decomposition reaction, at physiological pH, by mixing a solution of calcium nitrate tetrahydrate $Ca(NO_3)_2{\cdot}4H_2O$ (0.29 M) and a solution containing ammonium hydrogenphosphate and sodium bicarbonate (0.45 M $(NH_4)_2HPO_4$ and 0.71 M of $NaHCO_3$) as reported previously [44]. The calcium solution was poured rapidly into the phosphate and carbonate solution at room temperature (22 °C). The large excess of phosphate and carbonate ions used in this protocol had a buffering effect allowing the pH to stabilize at around 7.4. The suspension was left to mature at room temperature for 7 days without stirring (as in physiological conditions) and was then filtered on a Buchner funnel, thoroughly washed with deionized water, freeze-dried and stored in a freezer (−18 °C) so as to avoid any alteration of the apatite nanocrystals. The apatite powder was then sieved, and the size fraction in the range of 100–200 μm was used for all further adsorption experiments.

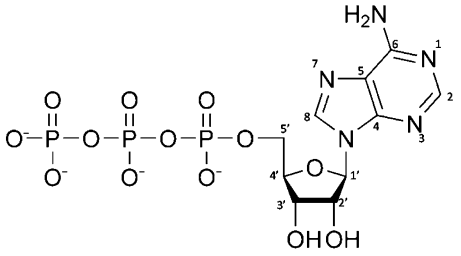

**Fig. 1.** Chemical formula of adenosine 5′ triphosphate (ATP)

The adenosine 5′ triphosphate (ATP) used in this study was provided by BIO BASIC Inc. in the form of ultrapure disodium salt trihydrate. The chemical formula of ATP is shown in Fig. 1.

### 2.2. Physico-chemical characterization

The solid phases were subjected to XRD, FTIR/Raman, TG-DTA analyses, as well as chemical titrations for Ca and inorganic phosphate, and scanning electron microscopy (SEM/EDX) observations. The details are as follows.

X-ray diffraction (XRD) analyses were performed on a CPS 120 INEL curved-counter powder diffractometer equipped with a graphite monochromator and using the Co Kα1 radiation (λ = 1.78892 Å). Mean crystallite lengths along the *c*-axis were estimated, in a first approximation, from the (0 0 2) line broadening using Scherrer's equation.

An FTIR (Thermo Nicolet 5700) spectrometer was used to study the vibrational features of the compounds. 2 mg of dried sample powder was compacted with 300 mg potassium bromide using a hydraulic pressure. For each spectrum, 64 scans between 400 and 4000 $cm^{-1}$ were recorded, with a resolution of 4 $cm^{-1}$.

Raman analyses of the samples, in the range 400–1800 $cm^{-1}$, were used for complementary vibrational spectroscopy analyses. Raman spectra were generated on a confocal Labram HR800 microspectrometer. The samples were exposed in backscattering mode to an AR-diode laser (λ = 532 nm) with a power of 17 mW. Measurements were carried out with a spectral resolution of 3 $cm^{-1}$. The uncertainty on Raman shifts (<1 $cm^{-1}$) have been calibrated using a silicon standard at 520.7 $cm^{-1}$. An optical objective 100× was used for all analyses, conferring to the system a lateral resolution of 0.7 μm and an axial resolution of 2.7 μm. The spectra reported in this work are the average of 3 spectral accumulations, each being exposed for 120 s.

The chemical composition of the apatite compound synthesized here was determined from titrations by complexometry for the determination of the calcium content, by spectrophotometry for the total phosphate content (determination of the sum of $PO_4^{3-}$ and $HPO_4^{2-}$ ions, using the phospho-vanado-molybdenic method [51] and by coulometry (UIC, Inc. CM 5014 coulometer with CM 5130 acidification unit) for the carbonate content.

Thermal analyses (TG-DTA) were performed using a Setaram Instrumentation SETSYS evolution system, with a heating rate of 5 °C/min, from 25 °C to 900 °C in air.

The specific surface area, $S_{BET}$, was determined using the BET method applied to nitrogen adsorption data recorded on a Tristar II Micromeritics apparatus.

Morphology and particle dimensions/agglomeration state of pure hac-7d and after adsorption of different amounts of ATP were followed using a scanning electron microscope (SEM) LEO 435 VP at a voltage of 15 kV, equipped with an EDX elemental analyzer.

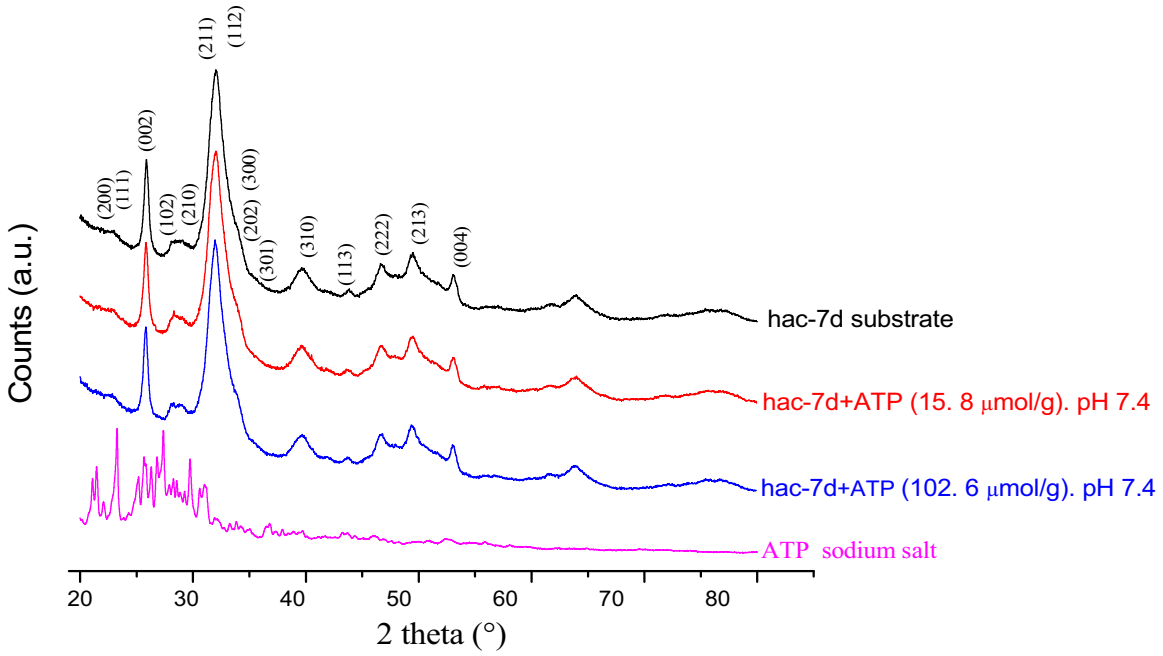


**Fig. 2.** XRD patterns ($2\theta$ between 20° and 80°) of the apatite substrate hac-7d before and after ATP adsorption for varying coverages, and XRD pattern for ATP (sodium salt). Numbers in parentheses refer to the Miller indices of crystallographic planes in reference to the JCPDS file #09-432 relative to hydroxyapatite

### *2.3. Adenosine triphosphate (ATP) adsorption*

For all adsorption experiments, 20 mg of apatite powder was dispersed in 5 ml of ATP solutions at room temperature. The ATP concentration present in the supernatant was evaluated by spectrophotometry (Shimadzu UV 1800, $\lambda = 259$ nm), and the adsorbed amount was determined by difference between the initial amount introduced in the medium and the residual amount in solution (supernatant after adsorption experiment).

The kinetics of adsorption was evaluated by following the amount of ATP adsorbed as a function of time, using an initial ATP concentration of 10 mM in KCl solution (0.01 M), at room temperature and physiological pH. Different contact times were checked, between 0 and 100 min to determine the minimum time needed to reach equilibrium. After the desired contact time, the mixture was centrifuged (10 min at 5000 rpm) and filtered on Millipore 0.2 μm, and the ATP concentration in the clear supernatant was determined by spectrophotometry as indicated above. The ATP adsorption isotherm was built by plotting the quantity of ATP adsorbed versus the equilibrium concentration.

## 3. Results and discussion

### *3.1. Physico-chemical characterization of the solids before and after ATP adsorption*

The X-ray diffraction (XRD) patterns obtained for the synthesized solid (Fig. 2), with or without adsorbed ATP, could be easily indexed by comparison of the JCPDS datasheet #09-432 relative to hydroxyapatite, with however broader peaks illustrating the low crystallinity of the prepared apatitic phase, as in bone mineral [11,29]. For these compounds, the XRD pattern obtained was thus found to be characteristic of single-phased apatite, as no secondary crystallized phase was detected. The mean crystallite length $L_{002}$ (along the *c*-axis of the apatite array) as approximated by Scherrer's formula [52] were systematically found close to 19–20 nm: these values are very analogous to those observed for bone samples [11,53].

The calcium, phosphate and carbonate contents were measured experimentally via EDTA complexometrey, visible spectrophotometry and coulometry, respectively. This led to a molar ratio Ca/(P + C) of the apatitic substrate of $1.36 \pm 0.02$ (carbonate weight percentage $\%CO_3$ of 3.6 wt.%). This value, significantly lower than 1.67 characteristic of stoichiometric hydroxyapatite (HA), points out the nonstoichiometric character of this apatitic substrate, as in bone mineral. Its specific surface area was $S_{BET} = 180\ m^2/g$.

The solids were then analyzed by vibrational spectroscopy techniques. The IR spectra of the apatite before and after adsorption with different amounts of ATP (reported in Fig. 3) present the characteristic bands of nonstoichiometric carbonated apatites [35,54,55]: in particular at 469 (attributable to the $\nu_2$ bending mode of $PO_4^{3-}$ groups), 535 (non-apatitic $HPO_4^{2-}$), 550 $cm^{-1}$ (apatitic $HPO_4^{2-}$), 562–576 and 603 ($\nu_4$ asymmetric bending of $PO_4^{3-}$ groups), 871–880 (P–OH vibration in $HPO_4^{2-}$ groups and $\nu_2$ bending mode of $CO_3^{2-}$), 959 ($\nu_1$ symmetric stretching of $PO_4^{3-}$ groups), 1030–1059 and 1098 ($\nu_3$ asymmetric stretching of $PO_4^{3-}$).

The bands observed at 1418, 1447 and 1474 $cm^{-1}$ are assignable to the $\nu_3$ vibration mode of carbonate groups [55]; the broad band at 1639 $cm^{-1}$ being attributable to water (bending mode) [56]. The band at 632 $cm^{-1}$ characteristic of apatitic $OH^-$ ions (librational mode) [54,55] was not clearly detectable on the spectra, indicating that this apatite sample was largely depleted in hydroxide ions: this type of nonstoichiometry is common for biological apatites [11,29], typically accompanied by cationic vacancies (lack of calcium ions) and the substitution of $PO_4^{3-}$ ions by divalent $HPO_4^{2-}$ or $CO_3^{2-}$.

Compared with the infrared spectrum of pure ATP sodium salt, the characteristic FTIR bands of the phosphate group of ATP generally observed between 509 and 1103 $cm^{-1}$ were covered by the vibration bands of the orthophosphate groups from the apatitic structure (mentioned above). The vibration broad band of the adenine part observed at 1711 $cm^{-1}$ [57] was also found to be overlapped with the broad water band at 1639 $cm^{-1}$, however the absorption spectrum showed a shoulder at 1259 $cm^{-1}$ assignable to the vibration $\nu_{as}(PO_2^-)$ in ATP [57]. We also note (Fig. 3b) the presence of additional weak bands about 1304 and 1335 $cm^{-1}$, while this new band does not seem to be present in the spectrum of ATP

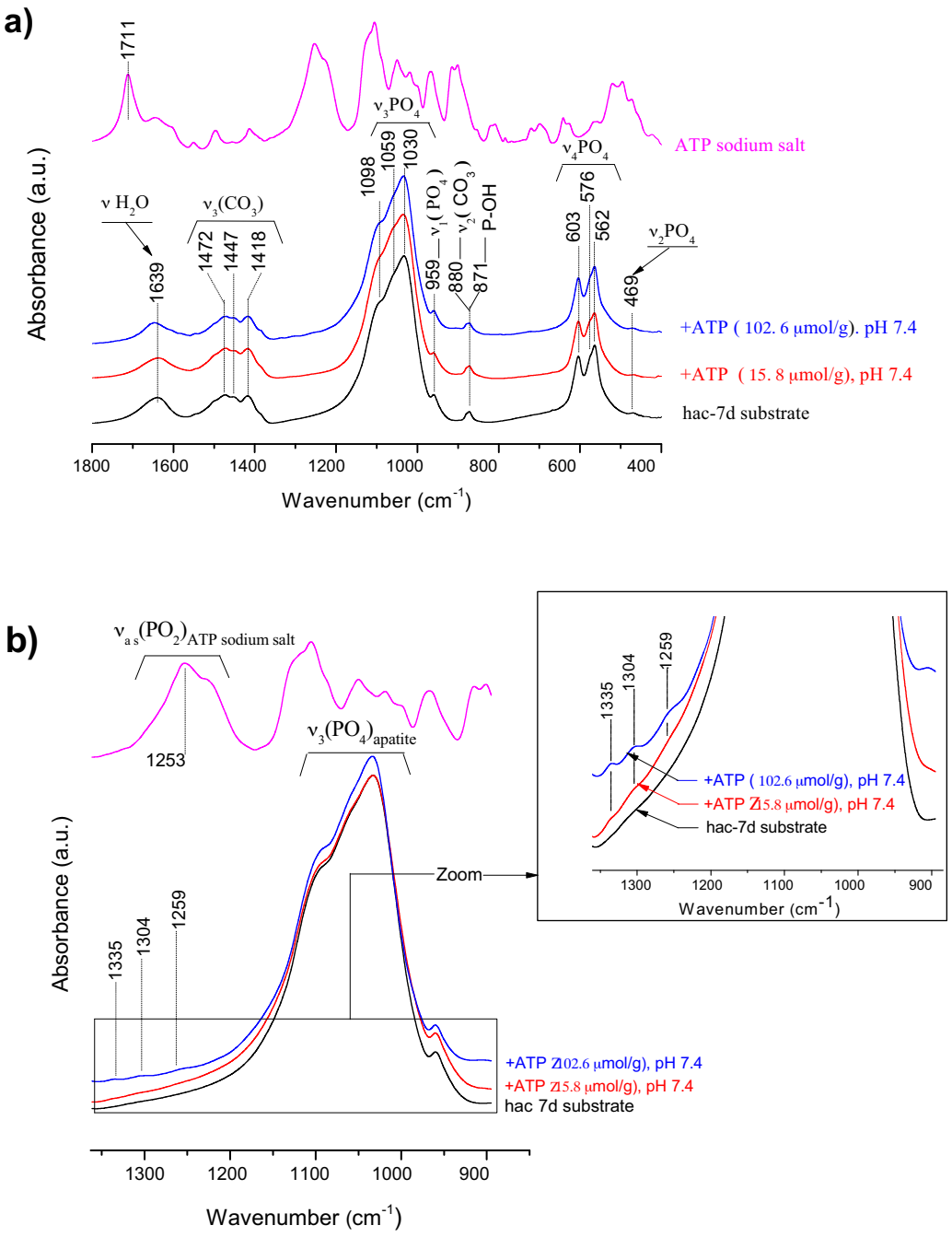


**Fig. 3.** (a) FTIR analysis of the apatitic substrate before and after ATP adsorption for varying coverages, and spectrum of ATP sodium salt. (b) Detail around the $\nu_3$ ($PO_4$) domain

sodium salt. In addition, the intensity of the new bands increases when increasing the amount of adsorbed ATP molecules on the surface of the hac-7d substrate. Since ATP molecules have negatively charged phosphate groups, but also lone pair of electrons on nitrogen atoms and $\pi$ electron clouds on adenine rings, therefore ATP may interact through these negatively charged moieties with positively charged surface sites (surface calcium ions) of the apatite substrate. The appearance of new bands seems to support this possibility. No significant change was noticed in the typical infrared frequencies of hac-7d, suggesting that the ATP molecules do not enter into the lattice of apatite nanocrystals nor affect significantly the vibrations of the crystalline core of apatite nanocrystals.

For a complementary vibrational spectroscopy analysis, Raman spectra were also recorded before and after adsorptive interaction with ATP. The Raman spectrum of the nanocrystalline carbonated apatite powders (Fig. 4a) showed characteristic lines of apatite phosphate groups [55,58] in accordance to the FTIR data, with typically the $\nu_1$ (960 $cm^{-1}$), $\nu_2$ (433, 448 $cm^{-1}$), the vibration domain $\nu_3$ (1029–1077 $cm^{-1}$) and the domain $\nu_4$ (580–614 $cm^{-1}$) of $PO_4^{3-}$. The band detected at 1071.3 $cm^{-1}$ was attributable to the $\nu_1$ vibration mode of type-B carbonate substitutions in apatite, although this line partly overlaps the $\nu_3$ mode of $PO_4^{3-}$.

Prominent Raman bands at about 701.8, 724.2 and 1323.5 $cm^{-1}$ in the Raman spectrum of ATP are assignable to out-of plane wagging of $NH_2$, ring-breathing of adenine ring and C5—N7 stretching, respectively [59] The Raman spectral region around this position appears significantly modified in the case of ATP adsorbed on biomimetic apatite, with a shoulder at 707.4 $cm^{-1}$ and a change

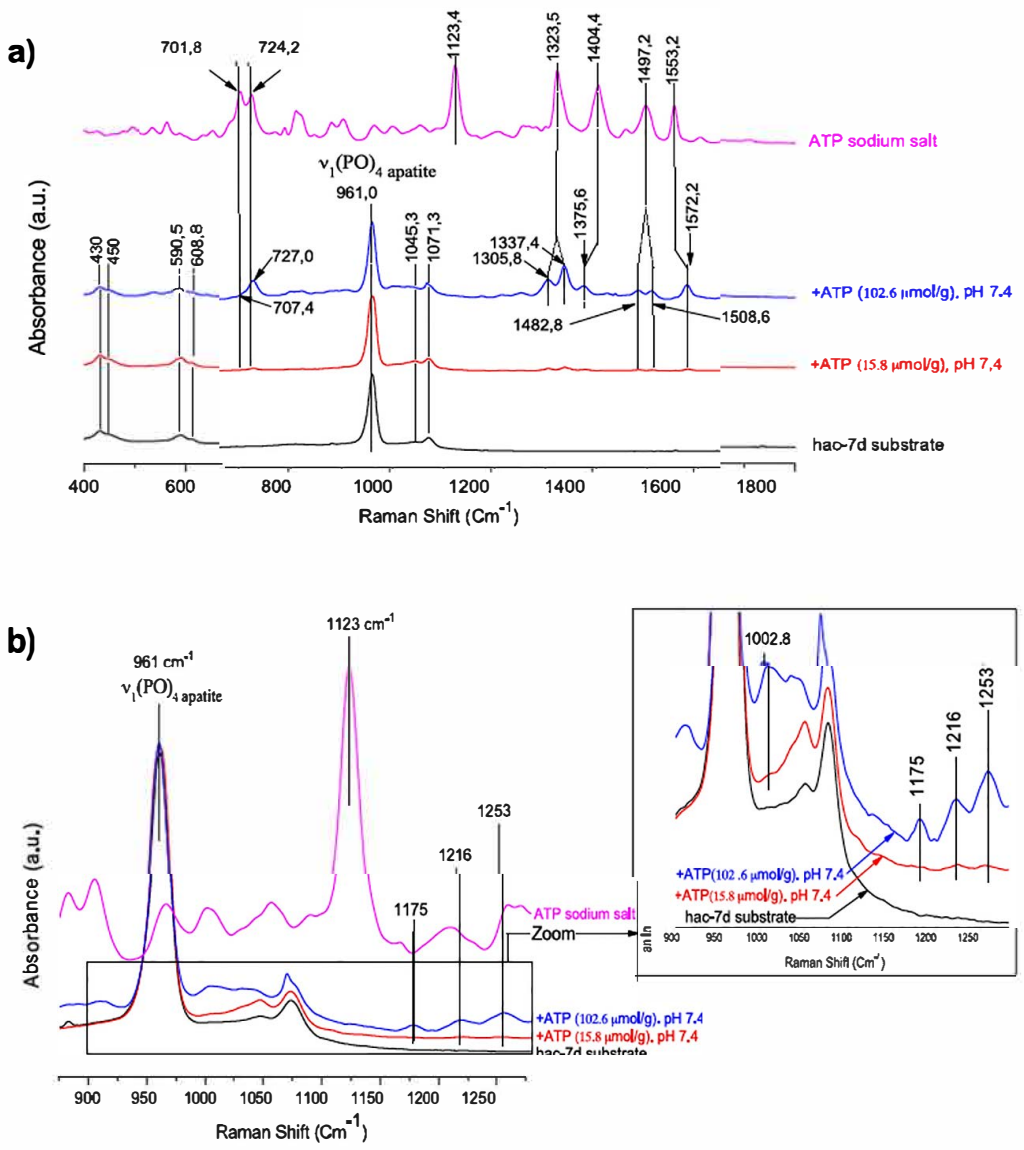


**Fig. 4.** Raman micro-spectroscopy analysisof the hac-7d substrate before or after adsorption (pH 7.4) and of ATP sodium salt: (a) general spectrum in the range 400–1800 $cm^{-1}$ and (b) zoom in the vibration region 900–1275 $cm^{-1}$

in the position of the second band to 727 $cm^{-1}$, while the latter band at 1323.5 $cm^{-1}$ gave way to two contributions near 1305.8 and 1337.4$cm^{-1}$. Furthermore, additional bands in the vibrational domain corresponding to the adenine ring are detectable, at about 1404.4 (assignable to C=N stretching mode) [59] and 1497.2 (assignable to C—N stretching mode) [60]: the position of the first band was shifted to 1375.6 $cm^{-1}$, while the latter band at 1497.2 $cm^{-1}$ was split into two peaks at 1588 and 1482.8 $cm^{-1}$ (doublet) in the hac-7d+ATP spectra. These findings support the fact that the adenine portion of the molecule takes part in the adsorptive process on apatite nanocrystals.

On the other hand, the triphosphate subunit of ATP is responsible for the presence of a rather strong Raman band located at 1123.4$cm^{-1}$ attributable to the vibration mode $\nu_1(O—P—O)_{ATP}$ [61]. Interestingly, in the 900-1275 $cm^{-1}$ spectral region, the Raman spectrum (Fig. 4b) appears significantly modified in the case of ATP adsorbed on apatite, with new bands detected at ca. 1175, 1216 and 1253 $cm^{-1}$ and no detection of the 1123 $cm^{-1}$ band, similarly to what was observed in the literature in the spectrum of ATP bound to a Au/CW substrate in a neutral environment (pH ≅ 7) [62]. These modifications indicate that the phosphate subunit of ATP is clearly involved also in the adsorption process. Note that the vibrations of apatitic phosphate were not fond to be significantly shifted upon ATP adsorption, probably due to the limited number of attached molecules.

In conclusion of this part, vibrational spectroscopy data (IR complemented by Raman) thus pointed out the existence of clear chemical interactions between ATP molecules and the surface of biomimetic apatite nanocrystals when contacted to each other. This adsorptive interaction not only involves the phosphate groups of ATP – as is often the case for phosphate-bearing molecules capable of interacting with surface calcium ions – but also the adenine part of the molecule. These findings can be compared to recent results on the adsorption of monophosphate nucleotides (AMP and CMP) [45,48] where both the phosphate end and the nucleic base were found to play a role in the sorption process on biomimetic apatite. Taking into account that adenine (present in AMP and ATP) is a puric base and cytosine (present in CMP) a pyrimidic base, this observation can probably be generalized to all nucleotides interacting with nanocrystalline apatite substrates.

In order to understand the thermal behavior of the apatitic substrate before and after ATP adsorption for varying coverages,

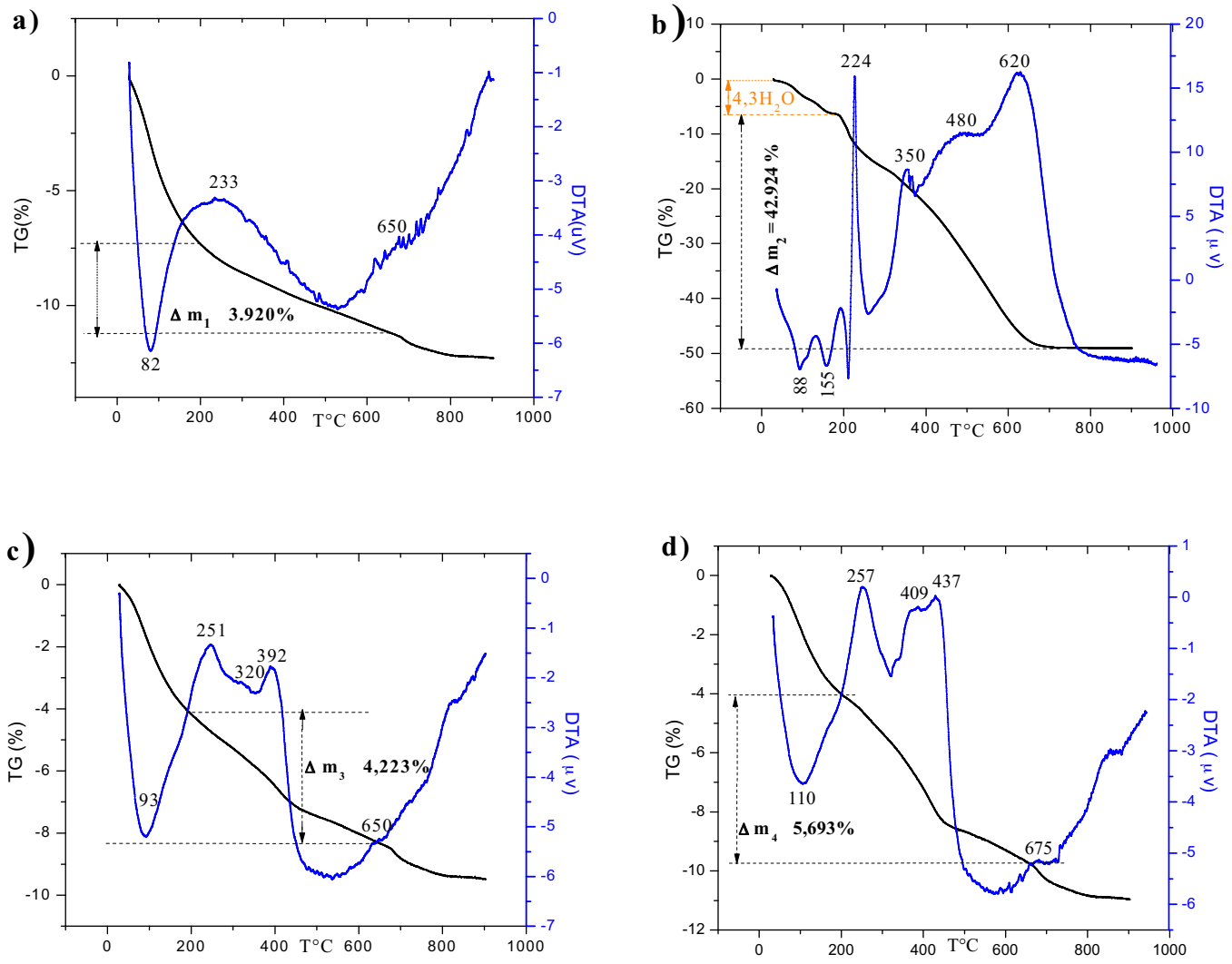


**Fig. 5.** TGA–DTA curves in air flow: (a) hac-7d, (b) ATP sodium salt, (c) hac-7d + 15.8 μmol/g of ATP, and (d) hac-7d + 102.6 μmol/g of ATP

thermogravimetric (TG) and differential thermal analysis (DTA) were carried out (Fig. 5). The TG curve obtained for the apatitic substrate alone (Fig. 5a) indicated the existence of three main weight losses. The first loss (8%), visible in the temperature range 25–250 °C was associated with the elimination of adsorbed water and water associated with the surface hydrated layer of the apatite nanocrystals. The second weight loss (2.45%) between 250 and 550 °C corresponds to the condensation of the hydrogenphosphate ions ($HPO_4^{2-}$) into pyrophosphate $P_2O_7^{4-}$ ions [63]. This fact is in accordance with the results of infrared spectroscopy indicating the presence of $HPO_4^{2-}$ ions. The third weaker weight loss (1%) occurs between 650 and 820 °C and can be attributed to the removal of carbon dioxide from the carbonated apatite and the reacting fraction of $P_2O_7^{4-}$ ions with the $OH^-$ ions present in the apatite structure in the hac-7d compound [64–66]. These weight losses are accompanied by corresponding peaks in the differential thermal analysis curve (Fig. 5a): the first peak presented an endothermic character with a maximum at 82 °C, while the other two peaks at 233 and 650 °C displayed were exothermic.

The TG curves of the ATP sodium salt (Fig. 5b) shows a small weight loss (6.14%) below 175 °C, resulting from the departure of 4.3 water molecules per formula unit. The second larger weight loss (42.92%) took place from 200 °C to 700 °C and can be attributed to the thermal decomposition of the organic part (ribose and adenine). The DTA curve of Fig. 5b showed two endothermic peaks at about 88 and 155 °C attributed to the first detected stage (dehydration of the salt), and four exothermic maxima at about 244, 350, 480 and 620 °C.

The TG curves obtained on the apatite substrate after ATP adsorption at two different coverages are represented in Fig. 5c and d. They indicate the existence of three different weight losses. The first loss, visible in the temperature range 25–190 °C was comprised between 4.21 and 4.02% and could be straightforwardly associated with the dehydration of the sample. Above 200 °C and up to 650 °C, a second degradation step was detected with weight losses of 4.22 and 5.69% for hac-7d associated to 15.8 μmol/g and 102.6 μmol/g of ATP, respectively. This second step can be attributed simultaneously to random scissions (thermal degradation) within the organic material and to the condensation of hydrogenphosphate ions into pyrophosphates. In the temperature range 200–650 °C, the TG curve for hac-7d displays a continuous weight loss corresponding to 3.92% inferior to 4.22 and 5.69%. These findings are in accordance with the amount of ATP linked to apatite. Again, this observation shows that hac-7d is a good adsorbent for this type of ribonucleotides. The last thermal event took place from 650 °C to 820 °C, displaying 1.02 and 1.08% weight losses for the two ATP/apatite samples respectively. This phenomenon was attributed to the carbonate decomposition and the reaction

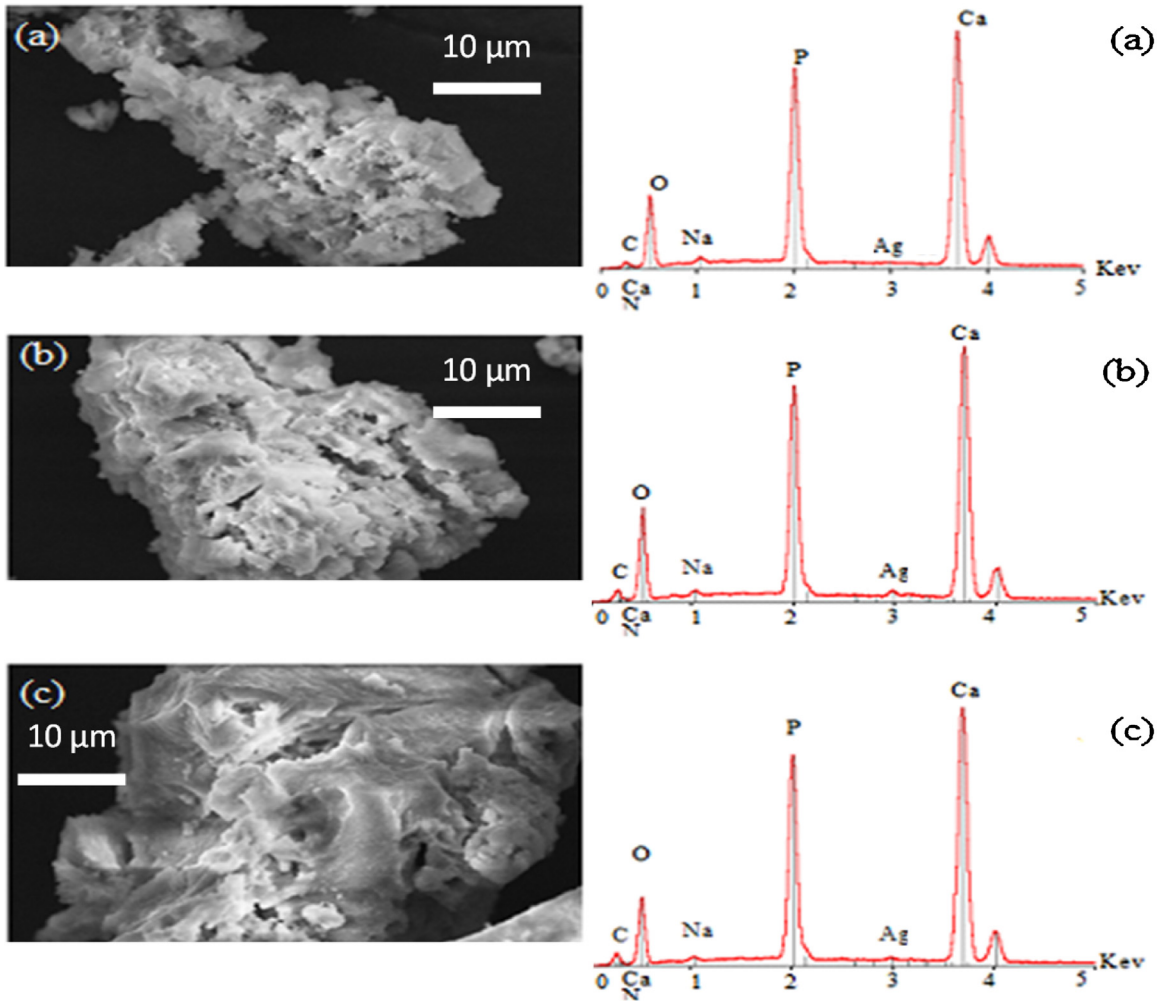


**Fig. 6.** SEM images and EDx spectra for (a) hac-7d, (b) hac-7d + 15.8 µmol/g of ATP and (c) hac-7d + 102.6 µmol/g of ATP

of $P_2O_7^{4-}$ ions with apatitic $OH^-$ ions present in the hac-7d network.

The DTA curves of the apatitic substrate after ATP adsorption for varying coverages show the presence of single endothermic peak observed at 90–110 °C, attributable to the desorption of water molecules. The manifold exothermic behavior observed between 250 and 437 °C corresponds to the combustion of the organic fraction of these samples. Finally, the exothermic peak at 650–800 °C is related to the decomposition of apatite as mentioned above.

Scanning electron microscopy analyses (SEM) were performed on the samples with or without ATP adsorption in view of direct observations of the substrate. The obtained micrographs (Fig. 6) showed the constitutive particles of the biomimetic apatite powder. Their morphology was not significantly altered by the adsorption of ATP. EDX spectra (Fig. 6) confirmed the presence of Ca, O, C and P elements on the samples analyzed as well as traces of Na (Ag was present only due to the silver metallization process prior to SEM analyses). Sodium being included in the precipitating medium as $NaHCO_3$ reagent, its presence as traces is not surprising, knowing the affinity of this element for the apatitic structure (also present in bone apatites).

### 3.2. ATP adsorption kinetics and isotherm

The kinetic follow-up of the adsorption process was carried out so as to determine the minimal amount of time necessary for the equilibration of the biomimetic apatite/ATP system in our working conditions (pH = 7.4, $T$ = 22 °C, [KCl] = $10^{-2}$ M). It revealed that the equilibrium on ATP adsorption by nanocrystalline apatite hac-7d was reached rapidly, in less than 30 min (Fig. 7a). In link with the small size of the ATP molecule (e.g. as compared to molecules such as DNA which require significantly larger equilibration times [44]) and the presence of phosphate endgroups, this short period of time illustrates the affinity of ATP molecules for the surface of biomimetic apatite.

Applying a contact time of 30 min to all subsequent adsorption experiments, the adsorption isotherm ($T$ = 22 °C) was then determined by modifying the initial ATP concentration, and the resulting plot is shown in Fig. 7b. The isotherm $N_{ads} = f(C_{eq})$, where $N_{ads}$ represents the adsorbed amount and $C_{eq}$ the equilibrated supernatant concentration, can be described by a first steep increase of the $N_{ads}$ versus $C_{eq}$ (up to ca. 0.1–0.2 mM) prolonged by a continuous increase of $N_{ads}$, although with a tendency to attenuate the tangent slope (see Fig. 7b).

In order to shed some more light on the type of adsorption behavior observed here between ATP molecules and biomimetic apatite crystals, several adsorption models were tentatively tested via mathematical treatment of the data. The Langmuir model, $N_{ads} = N_{max} \cdot K_L \cdot C_{eq} / (1 + K_L \cdot C_{eq})$ as well as Freundlich model, $N_{ads} = K_F \cdot C_{eq}^{1/n}$, were tested first because these variants are recurrently cited in the literature concerning adsorption on apatite compounds (e.g. [25,67,68]). Mathematical fitting led to correlation coefficients $R^2$ of 0.9755 and 0.9953 respectively. Keeping in mind that Freundlich model was initially established to take into account the

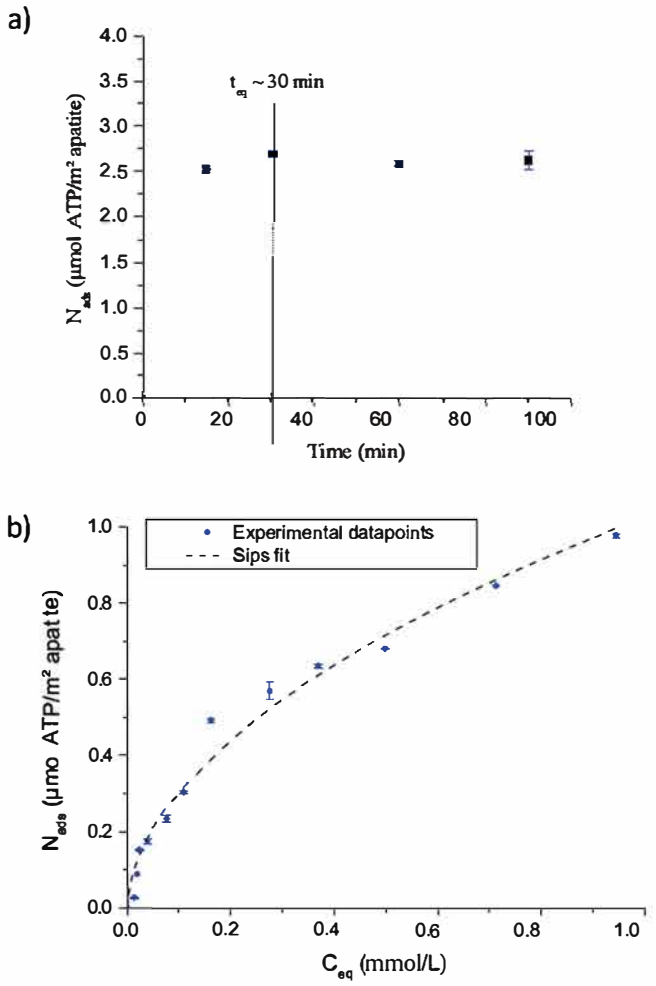


Fig. 7. (a) Kinetics of ATP adsorption from aqueous solutions by nanocrystalline carbonated apatite (hac-7d) and (b) adsorption isotherms of ATP on to (hac-7d) substrate. The dotted line corresponds to the fit using Sips model.

variability of surface sites (and corresponding adsorption energies) as opposed to Langmuir hypotheses considering all sites equivalent, the significantly better fit obtained with Freundlich equation suggests that the surface heterogeneity of apatite nanocrystals has to be taken into account in the discussion for understanding ATP adsorption.

However, recently we showed on various adsorption studies on nanocrystalline apatites [42,45,48] that the more general Sips model (also known as Langmuir–Freundlich or Hill isotherms) was often even more adapted to describe experimental adsorptive data. It was recently the case for describing the adsorption of adenosine monophosphate (AMP) [45] and for cytidine monophosphate (CMP) [48]. This model has the advantage to allow considering both the existence of surface heterogeneities (as for Freundlich) but also of interaction between adsorbed molecules; it thus appears well suited to model the adsorption of multifunctional molecules such as nucleotides on the heterogeneous surface of biomimetic apatite nanocrystals. This model reminds that of Langmuir, but with the use of an exponent "$m$" applied to the equilibrium concentration, leading to the equation:

$$N_{ads} = N_{max} \cdot \frac{K_S \cdot C_{eq}^m}{1 + K_S \cdot C_{eq}^m} \quad (1)$$

where $m$ is the Sips exponent, $N_{max}$ is the maximal coverage and $K_S$ is the Sips constant. As may be seen, this equation is equivalent to Langmuir's isotherm for the particular case where $m = 1$.

Interestingly, fitting the experimental data to the Sips model led to an improved correlation factor $R^2$ of 0.9964. Our findings thus indicate that, in the present case also, the adsorption data can be very satisfyingly described by a Sips isotherm. The fitted parameters were found as follows: $m = 0.56 \pm 0.05$, $K_S = 0.106 \pm 0.068$ (for $C_{eq}$ expressed in mmol/l), and $N_{max} = 10.7 \pm 5.9$ µmol/m$^2$.

Since similar Sips fits had previously been carried out for the adsorption of two monophosphate nucleotides AMP [45] and CMP [48] on similar carbonated nanocrystalline apatite substrates, it then became possible to compare their adsorptive behavior with that of ATP. As was mentioned in a previous study [45], even among monophosphate nucleotides some clear differences can be evidenced. Indeed, different couples of Sips parameters [$K_S$; $N_{max}$] have been obtained for AMP [1.14; 0.106 µmol/m$^2$] and for CMP [0.00052; 0.66 µmol/m$^2$] despite close values of $m$ (1.25 ± 0.45 for AMP and 1.20 ± 0.11 for CMP). These findings point out the non-negligible influence of the nucleic base, as confirmed by vibrational spectroscopy data. Interestingly, the Sips parameters determined here for the adsorption of ATP are [0.106; 10.7 µmol/m$^2$] and $m = 0.56 \pm 0.05$. Therefore, the value of the Sips constant $K_S$ in the case of ATP is found intermediate between those of AMP and CMP (although closer to that of AMP), but the maximum coverage is noticeably greater for ATP, and in particular systematically larger than for AMP whatever the concentration in solution. If we take for instance the example of an equilibrium concentration of 1 mmol/L, the obtained coverages $N_{ads}$ (at pH 7.4 and 22 °C) are ~1.03 µmol/m$^2$ for ATP to compare to ~0.056 µmol/m$^2$ for AMP [45] and ~0.254 µmol/m$^2$ for CMP [48]. Thus, despite a larger molecular size, ATP molecules tend to cover more efficiently the surface of biomimetic apatite nanocrystals than AMP or CMP. This can thus be related to the presence of the triple phosphate subgroup allowing more interactions with the substrate surface.

It may also be noticed that the value of $m$ found for ATP (0.56) is lower than that of AMP (1.25) and CMP (1.20), and even lower than unity. Contrarily to the cases of AMP or CMP, the exponent $m < 1$ suggests a situation where the adsorption of ATP molecules is not a cooperative process [69]: the adsorption behavior is thus probably more guided by the interaction between ATP and surface sites (favored by the long phosphate chain capable of interacting with several neighboring surface calcium ions as in the case of bisphosphonates [68]) than by intermolecular stabilization. In other words, our finding suggest that in the adsorption of mono-phosphate nucleotides such as AMP or CMP on biomimetic apatites, the affinity for the surface not only involves interactions between the molecules and the surface, but also cooperative interactions among adsorbed species; in contrast, ATP adsorption involves ATP/surface interaction, but is not favored by interactivity between adsorbed molecules.

From the value of $K_S$, it is possible to evaluate the *standard* Gibbs free energy associated to the adsorption process (as recently reminded with the example of tetracycline adsorption on biomimetic apatite [42]), using the following equation (with $C_{eq}$ re-expressed in mol/L):

$$K_S = \exp\left(-\frac{\Delta G^\circ_{ads}}{RT}\right) \quad (2)$$

Application of this equation to the case of ATP leads to the negative value $\Delta G^\circ_{ads} \cong -4$ kJ/mol (uncertainty estimated to ±2 kJ/mol). It is noticeably lower in absolute value than those found earlier, also in standard thermodynamic conditions, for the adsorption of CMP (−19 kJ/mol) and for AMP or tetracycline (−22 kJ/mol) on rather similar nanocrystalline apatite substrates. Although this order of magnitude found for ATP falls in what is generally considered as physisorption rather than chemisorption [70], the negative value tends to suggest however a rather favorable adsorption of ATP on

biomimetic apatite in standard conditions. Of even greater relevance is the *effective change* of free energy $\Delta G_{abs}$, which can be evaluated [71] for any condition corresponding to a concentration $C$ (mol/L) and an adsorbed amount $N_{ads}$ using the following relation:

$$\Delta G_{ads} = \Delta G^{\circ}_{ads} - mRT \cdot \mathrm{Ln}(C) + RT \cdot \mathrm{Ln}\left[\frac{N_{ads}}{N_{th} - N_{ads}}\right] \quad (3)$$

where $N_{th}$ is the maximum theoretical capacity, $T$ is the absolute temperature in Kelvin, $R$ is the gas constant ($8.314\,J\,mol^{-1}\,K^{-1}$), and $m$ is the Sips exponent. Assigning $N_{th} = N_{max}$, this equation then allows one to evaluate $\Delta G_{abs}$ along the adsorption process, which represents the *thermodynamic driving force* leading any $C_{ini}$ to reach the corresponding $C_{eq}$ accompanied by the adsorption of $N_{ads}$. As was previously done in the case of tetracycline adsorption onto biomimetic apatite [42], it is interesting to follow in particular the actual driving force (=value of $\Delta G_{abs}$) occurring when a small fraction of the total adsorption amount is reached – which thus corresponds to appoint near the initiation of the adsorption process. For example, $\Delta G_{ads}$ was found here to range between −29 and −33 kJ/mol when one thousandth (1/1000th) of the equilibrium adsorption amount was reached. Then, as this fraction increases (i.e. as the adsorption process progresses toward equilibrium, for any given $C_{ini}$), the value of $\Delta G_{ads}$ can be evaluated in a similar way. Interestingly, negative values of $\Delta G_{ads}$ were obtained throughout the whole ATP/apatite adsorption process, with values from −33 to 0 kJ/mol (0 kJ/mol being obtained at equilibrium). Thus, despite the small amplitude of $\Delta G^{\circ}_{ads}$ ($\cong$−4 kJ/mol), the very large value of $N_{max}$ (which is involved in Eq. (3)) compensates this effect and leads to significantly negative values of $\Delta G_{ads}$, indicating that the adsorption process is bound to spontaneously occur. Our vibrational data indicated indeed the existence of spectral modifications of ATP features upon adsorption, suggesting the existence of non-negligible interactions between ATP molecules and apatite nanocrystals.

### 3.3. Concluding remarks

The use of biomimetic apatite bonded to ATP molecules could have a variety of pharmacological, biological and technological applications taking into account (1) the direct effect of ATP on cells energetic pathways and (2) the interest of biomimetic apatites in biomedical applications due to their intrinsic biocompatibility. For this reason, it is of fundamental importance to study the interaction phenomena involved in the ATP/biomimetic apatite adsorption process.

Our experimental data indicate that ATP can adsorb effectively onto biomimetic apatite, and the isotherm can be satisfyingly described by the Sips equation as was observed previously for monophosphate nucleotides such as AMP. Despite a smaller value of the affinity constant $K_S$ and of the exponential factor $m$, larger adsorption values $N_{ads}$ were obtained for ATP as compared to AMP for any given concentration in solution. The value of $m$ lower than 1 suggests here a situation where intermolecular interactions are less favorable for ATP than with AMP, and the ATP/apatite adsorption appears to be mostly guided by direct interactions between ATP molecules and the surface of apatite nanocrystals.

On the basis of vibrational spectroscopy results (FTIR and Raman), it can be concluded that a clear chemical-like interaction is established between ATP molecules and the surface of apatite nanocrystals. In spite of a *standard* $\Delta G^{\circ}_{ads}$ estimated to only −4 kJ/mol, the large value of $N_{max}$ leads to significantly negative *effective* $\Delta G_{ads}$ values down to −33 kJ/mol, reflecting the spontaneous character of this ATP/apatite adsorption process. The affinity of the surface for ATP can probably be explained by the presence of the triphosphate group but the nucleic base was also found to get involved as modified vibrational features were observed upon adsorption.

Results of the present study are intended to serve as a basis for future research works involving ATP and apatite nanocrystals/nanoparticles in view of biomedical applications (e.g. bone tissue engineering, intracellular drug delivery, ...), especially by directly exploiting the presence of ATP which represents a source of energy for cells or for ATP-triggered drug delivery. In this view, future research will also include ATP release studies in various conditions. The fact that ATP, a key biomolecule, can efficiently adsorb onto apatite minerals may also be informative for investigations related to the development of life on primitive Earth. Indeed, through the adsorption process, biomolecules like ATP may have been "protected" against premature degradation (as was previously discussed in the case of DNA adsorption [44]), and allowed to undergo potentially catalyzed surface reactions [72].

## Acknowledgements

The authors thank the University of Sfax, Tunisia, for providing financial support to Mr. Khaled Hammami for a doctoral stay in France.

## References

[1] T. Forrester, A.R. Lind, Identification of adenosine triphosphate in human plasma and the concentration in the venous effluent of forearm muscles before, during and after sustained contractions, J. Physiol. 204 (1969) 347–364.
[2] F. Lipmann, Metabolic Generation and Utilization of Phosphate Bond Energy. Advances in Enzymology and Related Areas of Molecular Biology, John Wiley & Sons, Inc., 2006, pp. 99–162.
[3] J.C. Sowden, H.O.L. Fischer, The chemistry and metabolism of the compounds of phosphorus, Annu. Rev. Biochem. 11 (1942) 203–216.
[4] E. Gajewski, D.K. Steckler, R.N. Goldberg, Thermodynamics of the hydrolysis of adenosine 5′-triphosphate to adenosine 5′-diphosphate, J. Biol. Chem. 261 (1986) 2733–2737.
[5] R.A. Alberty, Thermodynamics of the hydrolysis of adenosine triphosphate as a function of temperature, pH, pMg, and ionic strength, J. Phys. Chem. B 107 (2003) 12324–12330.
[6] R. Mo, T.Y. Jiang, W.J. Sun, Z. Gu, ATP-responsive DNA–graphene hybrid nanoaggregates for anticancer drug delivery, Biomaterials 50 (2015) 67–74.
[7] H. Autefage, F. Briand-Mesange, S. Cazalbou, C. Drouet, D. Fourmy, S. Goncalves, J. Salles, C. Combes, P. Swider, C. Rey, Adsorption and release of BMP-2 on nanocrystalline apatite-coated and uncoated hydroxyapatite/beta-tricalcium phosphate porous ceramics, J. Biomed. Mater. Res. B 91 (2009) 706–715.
[8] C. Drouet, F. Bosc, M. Banu, C. Largeot, C. Combes, G. Dechambre, C. Estournes, G. Raimbeaux, C. Rey, Nanocrystalline apatites: from powders to biomaterials, Powder Technol. 190 (2009) 118–122.
[9] C. Drouet, J. Gomez-Morales, M. Iafisco, S. Sarda, Calcium phosphate surface tailoring technologies for drug delivering and tissue engineering, in: L. Rimondini, C.L. Bianchi, E. Vernè (Eds.), Surface Tailoring of Inorganic Materials for Biomedical Applications, Bentham Science, e-book, 2012, pp. 43–111.
[10] D. Eichert, C. Drouet, H. Sfihi, C. Rey, C. Combes, Nanocrystalline apatite-based biomaterials: synthesis, processing and characterization, in: J.B. Kendall (Ed.), Biomaterials Research Advances, Nova Science Publishers, 2007, pp. 93–143.
[11] J. Gomez-Morales, M. Iafisco, J. Manuel Delgado-Lopez, S. Sarda, C. Drouet, Progress on the preparation of nanocrystalline apatites and surface characterization: overview of fundamental and applied aspects, Prog. Cryst. Growth Charac. Mater. 59 (2013) 1–46.
[12] C. Rey, C. Combes, C. Drouet, H. Sfihi, A. Barroug, Physico-chemical properties of nanocrystalline apatites: implications for biominerals and biomaterials, Mater. Sci. Eng. C 27 (2007) 198–205.
[13] C. Rey, C. Combes, C. Drouet, D. Grossin, Bioactive ceramics: physical chemistry, in: P. Ducheyne, K.E. Healy, D.W. Hutmacher, D.W. Grainger, C.J. Kirkpatrick (Eds.), Comprehensive Biomaterials, vol. 1., Elsevier, 2011, pp. 187–221.
[14] C. Rey, C. Combes, C. Drouet, S. Cazalbou, D. Grossin, F. Brouillet, S. Sarda, Surface properties of biomimetic nanocrystalline apatites; applications in biomaterials, Prog. Cryst. Growth Charac. Mater. 60 (2014) 63–73.
[15] C.G. Weber, M. Mueller, N. Vandecandelaere, I. Trick, A. Burger-Kentischer, T. Maucher, C. Drouet, Enzyme-functionalized biomimetic apatites: concept and perspectives in view of innovative medical approaches, J. Mater. Sci.: Mater. Med. 25 (2014) 595–606.
[16] R. Bosco, M. Iafisco, J. van den Beucken, S. Leeuwenburgh, J. Jansen, Adsorption of alendronate onto biomimetic apatite nanocrystals to develop drug carrier coating for bone implants, Bioceramics 24 (529–530) (2013) 475–479.
[17] M. Iafisco, B. Palazzo, G. Martra, N. Margiotta, S. Piccinonna, G. Natile, V. Gandin, C. Marzano, N. Roveri, Nanocrystalline carbonate-apatites: role of

Ca/P ratio on the upload and release of anticancer platinum bisphosphonates, Nanoscale 4 (2012) 206–217.
[18] B. Palazzo, M. Iafisco, M. Laforgia, N. Margiotta, G. Natile, C.L. Bianchi, D. Walsh, S. Mann, N. Roveri, Biomimetic hydroxyapatite-drug nanocrystals as potential bone substitutes with antitumor drug delivery properties, Adv. Funct. Mater. 17 (2007) 2180–2188.
[19] R.Z. LeGeros, Calcium phosphate-based osteoinductive materials, Chem. Rev. 108 (2008) 4742–4753.
[20] Y.R. Cai, R.K. Tang, Calcium phosphate nanoparticles in biomineralization and biomaterials, J. Mater. Chem. 18 (2008) 3775–3787.
[21] C.S. Chai, B. Ben-Nissan, Bioactive nanocrystalline sol–gel hydroxyapatite coatings, J. Mater. Sci.: Mater. Med. 10 (1999) 465–469.
[22] A. Al-Kattan, F. Errassifi, A. Sautereau, S. Sarda, P. Dufour, A. Barroug, I. Dos Santos, C. Combes, D. Grossin, C. Rey, C. Drouet, Medical potentialities of biomimetic apatites through adsorption, ionic substitution, and mineral/organic associations: three illustrative examples, Adv. Eng. Mater. 12 (2010) B224–B233.
[23] A. Al-Kattan, S. Girod-Fullana, C. Charvillat, H. Ternet-Fontebasso, P. Dufour, J. Dexpert-Ghys, V. Santran, J. Bordere, B. Pipy, J. Bernad, C. Drouet, Biomimetic nanocrystalline apatites: emerging perspectives in cancer diagnosis and treatment, Int. J. Pharm. 423 (2012) 26–36.
[24] A. Al-Kattan, V. Santran, P. Dufour, J. Dexpert-Ghys, C. Drouet, Novel contributions on luminescent apatite-based colloids intended for medical imaging, J. Biomater. Appl. 28 (2014) 697–707.
[25] M. Iafisco, E. Varoni, M. Di Foggia, S. Pietronave, M. Fini, N. Roveri, L. Rimondini, M. Prat, Conjugation of hydroxyapatite nanocrystals with human immunoglobulin G for nanomedical applications, Colloids Surf. B: Biointerfaces 90 (2012) 1–7.
[26] M. Iafisco, J. Manuel Delgado-Lopez, E.M. Varoni, A. Tampieri, L. Rimondini, J. Gomez-Morales, M. Prat, Cell surface receptor targeted biomimetic apatite nanocrystals for cancer therapy, Small 9 (2013) 3834–3844.
[27] T. Welzel, I. Radtke, W. Meyer-Zaika, R. Heumann, M. Epple, Transfection of cells with custom-made calcium phosphate nanoparticles coated with DNA, J. Mater. Chem. 14 (2004) 2213–2217.
[28] D.C. Al-Kattan, A.M. Choimet, A. Tourrette, V. Santran, J. Dexpert-Ghys, B. Pipy, F. Brouillet, M. Tourbin, Biomimetic apatite-based functional nanoparticles as promising newcomers in nanomedicine: overview of 10 years of initiatory research, HSOA J. Gen. Pract. Med. Diagn. (GPMD) 1 (2015) 1–9.
[29] C. Rey, C. Combes, C. Drouet, M. Glimcher, Bone mineral: update on chemical composition and structure, in: 3rd Meeting on Bone Quality, vol. 20, 2009, pp. 1013–1021.
[30] T. Noro, K. Itoh, Biomechanical behavior of hydroxyapatite as bone substitute material in a loaded implant model. On the surface strain measurement and the maximum compression strength determination of material crash, Bio-Med. Mater. Eng. 9 (1999) 319–324.
[31] E. Ebaretonbofa, J.R.G. Evans, High porosity hydroxyapatite foam scaffolds for bone substitute, J. Porous Mater. 9 (2002) 257–263.
[32] Y.C. Liu, T. Wang, F.L. He, Q.A. Liu, D.X. Zhang, S.L. Xiang, S.P. Su, J.A. Zhang, An efficient calcium phosphate nanoparticle-based nonviral vector for gene delivery, Int. J. Nanomed. 6 (2011) 721–727.
[33] V.V. Sokolova, I. Radtke, R. Heumann, M. Epple, Effective transfection of cells with multi-shell calcium phosphate-DNA nanoparticles, Biomaterials 27 (2006) 3147–3153.
[34] G. Montel, G. Bonel, J.C. Heughebaert, J.C. Trombe, C. Rey, New concepts in the composition, crystallization and growth of the mineral component of calcified tissues, J. Cryst. Growth 53 (1981) 74–99.
[35] H. Elfeki, C. Rey, M. Vignoles, Carbonate ions in apatites – infrared investigations in the nu-4 $CO_3$ domain, Calcified Tissue Int. 49 (1991) 269–274.
[36] C. Rey, J. Lian, M. Grynpas, F. Shapiro, L. Zylberberg, M.J. Glimcher, Non-apatitic environments in bone mineral: FT-IR detection, biological properties and changes in several disease states, Connect. Tissue Res. 21 (1989) 267–273.
[37] C. Rey, B. Collins, T. Goehl, I.R. Dickson, M.J. Glimcher, The carbonate environment in bone-mineral – a resolution enhanced Fourier-transform infrared-spectroscopy study, Calcified Tissue Int. 45 (1989) 157–164.
[38] C. Rey, M. Shimizu, B. Collins, M.J. Glimcher, Resolution-enhanced Fourier-transform spectroscopy study of the environment of phosphate ions in the early deposits of a solid-phase of calcium-phosphate in bone and enamel, and their evolution with age. 1. Investigations in the $\nu_4$ $PO_4$ domain, Calcified Tissue Int. 46 (1990) 384–394.
[39] C. Rey, V. Renugopalakrishnan, B. Collins, M.J. Glimcher, Fourier-transform infrared spectroscopic study of the carbonate ions in bone mineral during aging, Calcified Tissue Int. 49 (1991) 251–258.
[40] N. Vandecandelaere, C. Rey, C. Drouet, Biomimetic apatite-based biomaterials: on the critical impact of synthesis and post-synthesis parameters, J. Mater. Sci.: Mater. Med. 23 (2012) 2593–2606.
[41] S. Cazalbou, D. Eichert, X. Ranz, C. Drouet, C. Combes, M.F. Harmand, C. Rey, Ion exchanges in apatites for biomedical application, J. Mater. Sci.: Mater. Med. 16 (2005) 405–409.
[42] S. Cazalbou, G. Bertrand, C. Drouet, Tetracycline-loaded biomimetic apatite: an adsorption study, J. Phys. Chem. B (2015).
[43] C. Drouet, M.-T. Carayon, C. Combes, C. Rey, Surface enrichment of biomimetic apatites with biologically-active ions $Mg^{2+}$ and $Sr^{2+}$: a preamble to the activation of bone repair materials, Mater. Sci. Eng. C 28 (2008) 1544–1550.
[44] A. Grunenwald, C. Keyser, A.M. Sautereau, E. Crubezy, B. Ludes, C. Drouet, Adsorption of DNA on biomimetic apatites: toward the understanding of the role of bone and tooth mineral on the preservation of ancient DNA, Appl. Surf. Sci. 292 (2014) 867–875.
[45] K. Hammami, H.E. Feki, O. Marsan, C. Drouet, Adsorption of nucleotides on biomimetic apatite: the case of adenosine 5′ monophosphate (AMP), Appl. Surf. Sci. 353 (2015) 165–172.
[46] N. Vandecandelaere, F. Bosc, C. Rey, C. Drouet, Peroxide-doped apatites: preparation and effect of synthesis parameters, Powder Technol. 255 (2014) 3–9.
[47] I. Rodriguez-Ruiz, J. Manuel Delgado-Lopez, M.A. Duran-Olivencia, M. Iafisco, A. Tampieri, D. Colangelo, M. Prat, J. Gomez-Morales, pH-responsive delivery of doxorubicin from citrate-apatite nanocrystals with tailored carbonate content, Langmuir 29 (2013) 8213–8220.
[48] M. Choimet, A. Tourrette, C. Drouet, Adsorption of nucleotides on biomimetic apatite: the case of cytidine 5′ monophosphate (CMP), J. Colloid Interface Sci. 456 (2015) 132–137.
[49] P. Pascaud, F. Errassifi, F. Brouillet, S. Sarda, A. Barroug, A. Legrouri, C. Rey, Adsorption on apatitic calcium phosphates for drug delivery: interaction with bisphosphonate molecules, J. Mater. Sci.: Mater. Med. 25 (2014) 2373–2381.
[50] K. Hammami, J. Elloumi, S. Aifa, C. Drouet, H. El Feki, Synthesis and characterization of hydroxyapatite ceramics organofunctionalized with ATP (adenosine triphosphate), J. Adv. Chem. 9 (2014) 1787–1797.
[51] A. Gee, V.R. Dietz, Determination of phosphate by differential spectrophotometry, Ann. Chem. 25 (1953) 1320–1324.
[52] A.L. Patterson, The Scherrer formula for X-ray particle size determination, Phys. Rev. 56 (1939) 978–982.
[53] A. Boskey, Bone mineral crystal size, Osteoporos. Int. 14 (2003) S16–S20.
[54] C. Drouet, Apatite formation: why it may not work as planned, and how to conclusively identify apatite compounds, Biomed. Res. Int. (2013) 12, Article ID 490946.
[55] C. Rey, O. Marsan, C. Combes, C. Drouet, D. Grossin, S. Sarda, Characterization of calcium phosphates using vibrational spectroscopies, in: B. Ben-Nissan (Ed.), Advances in Calcium Phosphate Biomaterials, vol. 2, Springer, Berlin, Heidelberg, 2014, pp. 229–266.
[56] R.Z. Legeros, G. Bonel, R. Legros, Types of $H_2O$ in human enamel and in precipitated apatites, Calcified Tissue Res. 26 (1978) 111–118.
[57] M. Matthies, G. Zundel, Hydraiton and self-association of adenosine triphosphate, adenosine diphosphate, and their 1=1 complexes with magnesium (II) at various pH values – infrared investigations, J. Chem. Soci. Perkin Trans. 2 (1977) 1824–1830.
[58] G. Penel, G. Leroy, C. Rey, E. Bres, MicroRaman spectral study of the $PO_4$ and $CO_3$ vibrational modes in synthetic and biological apatites, Calcified Tissue Int. 63 (1998) 475–481.
[59] A. Lanir, N.T. Yu, Raman spectroscopic study of the interaction of divalent metal ions with adenine moiety of adenosine 5′ triphosphate, J. Biol. Chem. 254 (1979) 5882–5887.
[60] T. Tenorio, A.M. Silva, J.M. Ramos, C.D. Buarque, J. Felcman, Molecular structure of tetraaqua adenosine 5′-triphosphate aluminium(III) complex: a study involving Raman spectroscopy, theoretical DFT and potentiometry, Spectrochim. Acta Part A: Mol. Biomol. Spectrosc. 105 (2013) 88–101.
[61] L. Rimai, T. Cole, J.L. Parsons, J.T. Hickmott Jr., E.B. Carew, Studies of Raman spectra of water solutions of adenosine tri-, di-, and monophosphate and some related compounds, Biophys. J. 9 (1969) 320–329.
[62] H. Fang, H.J. Yin, M.Y. Lv, H.J. Xu, Y.M. Zhao, X. Zhang, Z.L. Wu, L. Liu, T.W. Tan, Approach for determination of ATP:ADP molar ratio in mixed solution by surface-enhanced Raman scattering, Biosens. Bioelectron. 69 (2015) 71–80.
[63] J.C. Heughebaert, Contribution à l'étude de l'évolution des orthophosphates de calcium précipités en orthophosphates apatitiques. vol. PhD., Institut National Polytechnique de Toulouse, Toulouse, France, 1977.
[64] M. Banu, vol. Ph.D., Institut National Polytechnique de Toulouse (INPT), Toulouse, France, 2005.
[65] D. Tadic, F. Peters, M. Epple, Continuous synthesis of amorphous carbonated apatites, Biomaterials 23 (2002) 2553–2559.
[66] E. Tkalcec, J. Popovic, S. Orlic, S. Milardovic, H. Ivankovic, Hydrothermal synthesis and thermal evolution of carbonate-fluorhydroxyapatite scaffold from cuttlefish bones, Mater. Sci. Eng. C: Mater. Biol. Appl. 42 (2014) 578–586.
[67] L. Benaziz, A. Barroug, A. Legrouri, C. Rey, A. Lebugle, Adsorption of O-phospho-L-serine and L-serine onto poorly crystalline apatite, J. Colloid Interface Sci. 238 (2001) 48–53.
[68] P. Pascaud, P. Gras, Y. Coppel, C. Rey, S. Sarda, Interaction between a bisphosphonate, tiludronate, and biomimetic nanocrystalline apatites, Langmuir 29 (2013) 2224–2232.
[69] L.K. Koopal, W.H. Vanriemsdijk, J.C.M. Dewit, M.F. Benedetti, Analytical isotherm equations for multicomponent adsorption to heterogeneous surfaces, J. Colloid Interface Sci. 166 (1994) 51–60.
[70] M.A. Al-Anber, in: J.C. Moreno-Pirajan (Ed.), Thermodynamics – Interaction Studies – Solids, Liquids and Gases, InTech, 2011, pp. 737–764.
[71] Y. Liu, Biosorption isotherms, kinetics and thermodynamics, Sep. Purif. Technol. 61 (2008) 229–242.
[72] F.G. Burton, M.W. Neuman, W.F. Neuman, On the possible role of crystals in the origins of life. I. The adsorption of nucleosides, nucleotides and pyrophosphate by apatite crystals, Biosystems 3 (1969) 20–26.